Leveraging Nanoscale Plasmonic Modes to Achieve Reproducible Enhancement of Light

Ryan T. Hill[1], Jack J. Mock[2, 3], Yaroslav Urzhumov[2, 3], David S. Sebba[4], Steven J. Oldenburg[4], Shiuan-Yeh Chen[2, 5], Anne A. Lazarides[1, 3, 5], Ashutosh Chilkoti[1, 6], and David R. Smith[2, 3]*

[1]Center for Biologically Inspired Materials and Material Systems (CBIMMS), Duke University, Box 90271, Durham, NC, 27708. [2]Department of Electrical and Computer Engineering, Duke University, Box 90201, Durham, NC, 27708. [3]Center for Metamaterials and Integrated Plasmonics (CMIP), Duke University, Box 90271, Durham, NC, 27708. [4]nanoComposix, Inc., 4878 Ronson Ct., Suite K, San Diego, CA, 92111. [5]Department of Mechanical Engineering and Materials Science, Duke University, Box 90300, Durham, NC, 27708. [6]Department of Biomedical Engineering, Duke University, Box 90281, Durham, NC, 27708

[*]To whom correspondence should be addressed. Email: drsmith@ee.duke.edu

Supporting Information

Gold Nanoparticle Preparation

Malachite green isothiocyanate (MGITC) functionalized gold nanoparticles (NPs) were prepared by nanoComposix, Inc. (San Diego, CA, USA). Briefly, 13.5 μL of aqueous, 45 μM MGITC (Invitrogen M689, concentration based on extinction coefficient of 150,000 L/mol*cm at 616.5 nm, Figure S1C) was incubated with 1 mL of 0.005 mg/mL of 60 nm nominal diameter BioPure™ gold NPs (nanoComposix: 57.9 nm mean diameter, 11.3% coefficient of variation, peak extinction at 531 nm, Figures S1A and S1B) for 2 hours, at which point the ensemble SERRS signal (Figure S1D) reached a steady state and was found to be stable for multiple days. Bulk Raman scattering of the MGITC-NPs was confirmed using a Raman spectrometer that consisted of a free space laser coupled to an optical fiber (633 nm, Melles Griot, CeramOptec multimode fiber) for light delivery, and a second collection multimode optical fiber (CeramOptec) coupled to an imaging spectrograph (Holospec f/1.8 Kaiser), which dispersed the collected light and imaged it onto an electron multiplied CCD detector (Newton, Andor) after Rayleigh scattering was removed using a holographic notch filter (633 nm, Semrock).

Given that there is an excess of 149,000 dye molecules per NP in solution, we assume maximum packing density of MGITC on all the NPs in solution. The assumption is supported by the fact that a previous report[1] observed MGITC to have a packing density such that each molecule occupies 1 nm^2 on a planar surface with monolayer molecular coverage. If we assume the same packing density for a spherical surface, it would take ~11,000 MGITC molecules to pack the surface area of each NP, which is calculated to be ~11,000 nm^2. Thus, we have roughly a factor of 14 more than the necessary MGITC molecules/NP required for maximum packing density. We believe this excess of MGITC should be enough to account for slight differences in MGITC packing density on a curved surface as compared to a planar surface.

NP-film Gap Preparation

Gold films and polyelectrolyte (PE) spacer layers were prepared and characterized as described previously.[2] Briefly, 45 nm gold films were deposited by an electron beam evaporator (CHA Industries) at 2 Angstroms/sec onto clean room cleaned Nexterion Glass B slides (Schott North America, Inc.) using a 5 nm chromium adhesion layer (deposited at 1 angstrom/sec). Layer-by-layer (LBL) deposition[3] of poly(allylamine) hydrochloride (PAH, M_w = 70 kDa, Aldrich) and polystyrene sulfonate (PSS, M_w = 70 kDa, Aldrich) was used to create PE spacer layers. For each deposition step, the gold-coated glass slides were immersed in 0.003 moles-of-monomer/L (monomol/L) PE and 1 M NaCl for 30 min, rinsed thoroughly with a gentle stream of ultra-pure water (18 MΩ, used throughout), and immersed in fresh ultra-pure water for 1 min, after which, the substrates were either immersed in 1 M NaCl for 30 s before repeating the same steps for deposition of the oppositely charged PE or dried with a stream of nitrogen for analysis and further use in NP-film surface-enhanced resonant Raman scattering (SERRS) studies. All LBL depositions were initiated and terminated with the cationic PAH layer to facilitate both the attachment of the first PE layer to the gold film through amine-gold interactions[4] and the electrostatic immobilization of gold nanoparticles to the PE spacer layer. NP-film gaps were created by electrostatically immobilizing MGITC-NPs on the top surfaces of each PE spacer layer. 100-µL drops of MGITC-NPs, diluted 1:1 with ultra-pure water, were applied to each PE-funtionalized gold film for 10 mins, followed by rinsing with ultra-pure water and drying under a stream of nitrogen.

NP-film Gap Distances

NP-film gap distances were assumed to be the sum of the PE spacer thickness, as measured by ellipsometry, and the height of a single MGITC molecular layer when immobilized to a gold surface. Previous reports[1] suggest that MGITC assembles on a planar gold surface at an inclined orientation and extends roughly 1 nm above the surface. We assumed the same MGITC monolayer thickness for the

case that MGITC is assembled onto 60-nm gold colloid. We note, however, that the MGITC molecular orientation, and hence layer height, on a curved surface is likely to be slightly different than what was observed on planar gold. We also note that there is a possibility that the MGITC molecules, in reality, may become slightly embedded within the PE layer.

PE spacer layer thicknesses were measured using a J.A. Woolam Co., Inc., M-88 spectroscopic ellipsometer and WVASE32 software (version 3.460). Spectroscopic scans (277.5 – 763 nm) of each PE spacer layer were performed in three distinct regions (free of immobilized NPs) at 65°, 70°, and 75° relative to the normal of the surface of the slide. Ellipsometry data was analyzed using a 2-layer model[5] composed of a bulk gold layer underneath an organic layer, which was used to represent the PE layer. The thickness of each PE spacer layer was fitted using the Cauchy expression for a normal dispersion.[6] For each PE spacer layer, the nominal thickness was determined to be the average of the three thickness measurements taken per spacer layer. Note that the optical constants of each bare gold film were determined immediately prior to LBL depositions by taking spectroscopic scans of the bare gold films at 65°, 70°, and 75° and fitting *n* and *k* to the known values of bulk gold, which were provided by the WVASE32 software, to account for any shifts in the optical constants due to the thicknesses of our gold films. These fitted optical constants for each gold slide were saved and used later, respectively, when fitting for thickness of the PE layers deposited onto the gold slides. Measured PE spacer thickness versus number of layers is plotted in Figure S2.

Simulations

The numerical simulation of the NP-film system is carried out using the Finite Element Method implemented in COMSOL Multiphysics with RF Module. The full-wave, frequency-domain equation for the electric field is used. The simulated domain is a sphere of radius 300 nm, surrounded by spherical Perfectly Matched Layers. The NP is modeled as a perfect sphere of radius 30 nm. The excitation is a plane wave with a pure P-polarization, incident at an angle 75° from the normal direction

of the substrate. To reduce the simulation time, a symmetry plane parallel to the wave vector of incident wave is used.

To better approximate the behavior of the infinitely thick substrate and the infinitely extended metal film, we use a scattered-field formulation, in which the background field is specified using an analytical formula, and the physical field is defined as the sum of the background and scattered field. For the background field, we use Fresnel formulas for a layered system consisting of a semi-infinite layer of air (refractive index n = 1), 45 nm thick layer of metal (wavelength-dependent refractive index from Johnson & Christy[7]), and a semi-infinite layer of glass (n = 1.47). Thus, the background field in the air consists of an incident plane wave of unit amplitude and the reflected wave with the amplitude calculated from Fresnel formulas; the background field in metal is a superposition of two waves, and in the glass substrate it is only the transmitted plane wave. The model also includes a flat layer of the polyelectrolyte, modeled as a lossless dielectric with n = 1.4; the sphere representing the NP touches this layer at exactly one point.

The scattering cross-section is obtained by evaluating the scattered Poynting flux, $Psc = 1/2\ Re(E_{sc} \times H_{sc}^*)$, integrating it over a range of spherical angles corresponding to numerical aperture NA = 0.9 ($NA = n_{air}*\sin(\theta_{max})$), and normalizing the result by the flux of the incident plane wave. Using a benchmark model of a single NP in air (without the substrate), we have verified that this approach gives very accurate scattering cross-sections in comparison with the analytical Mie solution.

The volume of our simulated SERRS hotspot at NP-film gap distance of 1.7 nm (633 nm DF illumination) was calculated to be the region occupied by field enhancements greater than the half-maximum of $(E/E_0)^4$. This volume corresponded to roughly 1 nm^3. Given that the volume of a single MGITC molecule is roughly 0.24 nm^3[3(1)], a maximum of 4-5 MGITC molecules could theoretically occupy our calculated hotspot volume. We note, however, that the number of MGITC molecules in our hotspot is also affected by the packing density of MGITC on our NP surfaces (see description above), which could reduce the number of molecules in the hotspot. Thus, we estimate that our SERRS signal

from single film-coupled NPs is likely coming from 1 – 5 MGITC molecules. This variation likely affects the variation in experimentally observed SERRS enhancement reported in Figure 3A.

Plasmonic Characterization of MGITC-Au NPs near Gold Film

MGITC-NPs near gold film were plasmonically characterized by single NP scattering spectra (Figure S3A) and color images (Figure 2A), ensemble-mode extinction spectra (Figure S3B), and numerical simulations (Figure 2C). Single NP scattering spectra and color images were acquired as described previously.[2] Briefly, NPs were imaged and their spectra taken using a customized Nikon darkfield (DF) microscope with a 100x DF 0.9 NA objective. Slides containing the gold films with immobilized spacer layers and NPs were index matched with oil to the top surface of a dove prism. Samples were illuminated from above using un-polarized white light from a 75 W Xenon lamp in DF mode. For color images, the microscope light path was directed to a Nikon d90 color camera used for color imaging. Single NP spectra were acquired using an adjustable pinhole aperture to reduce the field of view to that of a single NP, which greatly reduces background signal in the imaging path. This field of view was directed through a spectrometer (Acton 2300SPI) and onto a detector (Photometrics CoolSnap HQ). All single NP spectra were background corrected by subtracting the spectrum from an apertured region of the substrate containing no NPs and normalized to correct for the wavelength response of the imaging system. At each NP-film gap distance, 10 single NP spectra were collected. Representative spectra from single NPs at each gap distance are shown in Figure S3A. Single NP localized surface plasmon resonance (LSPR) peak positions from each of the 10 NPs at each gap distance were identified by finding the centroid of the top 25% of each peak. The average LSPR versus NP-film gap distance is plotted in Figure S3C.

Extinction measurements from NPs near film (Figure S3B) were made using a J.A. Woollam M-88 spectroscopic ellipsometer in reflectivity mode at 70° using P-polarized light. S-polarized light was also used (data not shown), but response from the NPs near film was too weak to measure (see discussion below). Extinction spectra represent the ratio of reflectivity from a spot on the gold film

containing a PE spacer and many immobilized NPs to that of a spot on the gold film containing only the PE spacer layer. For this reason, the extinction of the NPs near film appear as dips in the plotted data, indicating that incident light reflected off the surface and directed at the detector is being both absorbed and scattered in all directions by NPs. No attempt was made to maintain the same surface coverage of NPs from sample to sample, and so differences in intensity should not be interpreted from this data. Extinction resonances were found by finding the centroid of the bottom 25% of each dip. These are plotted versus NP-film gap distance in Figure S3C.

NP scattering efficiency from NPs near film (Figure 2C) was also simulated using a numerical model, which is described above. The simulated NP LSPR versus NP-film gap distance is also plotted in Figure S3C.

Plasmonic characterization using single NP LSPR scattering spectra, ensemble extinction spectra, and simulations all indicate blue shifting of the NP-film plasmon resonance as the NPs are spaced further away from the underlying gold film. We note, however, significant differences in trends in peak position with gap distance between extinction and scattering and between simulation and experiment. For all NP-film gaps studied, the wavelength of maximum scattering is between 15 and 40 nm to the red of the wavelength of max extinction. In general, peak scattering is offset from peak extinction when an electric dipole resonance is shifted beyond the spectral range where absorption is significant. For gold NPs in solution this occurs only for particles significantly larger than the particles studied here.[8,9] From our data it appears that coupling of the NP to the gold film similarly shifts the scattering beyond the spectral range of high absorbance. We also find for all except the most weakly coupled (most widely spaced) NP-film scatterers that the position of peak scattering is also 10's of nanometers to the red of the scattering maxima from simulation. For peaks to the red of the MGITC absorbance max, this can be attributed to the polarizability of the fluorophores, a phenomenon not included in the NP-film model simulated here.[10] However, the difference between positions of measured and simulated scattering bands at shorter wavelengths is less easy to understand. While there are other bluer bands in the MGITC spectrum, which may contribute to the polarizability of the environment at lower frequencies, a number

of other idealizations in the model may play a role. Among these is the assumption that the metal film has the full conductivity of bulk gold, an assumption that may overestimate the extent to which the substrate nulls the short wavelength horizontal dipole, which is green. Our model is still being refined in order to consider both local and non-local effects on the electronic oscillations in the gold NP-film, which might shift the resonant frequency, somewhat. A more refined model of these subtler effects remains for future work.

SERRS Characterization of MGITC-NPs near Gold Film

Viewing surface-enhanced resonant Raman scattering (SERRS) from the MGITC-NP-film gaps required illumination with a 3 mW 633 nm HeNe laser line. This was accomplished in two different ways: in DF mode and in total internal reflection (TIR) mode. TIR mode was necessary to facilitate introduction of the laser illumination into the microscope imaging system, while maintaining the ability to acquire high-resolution SERRS signal from single NP-film gaps using a short working distance 100x 0.9 NA DF objective. Here, TIR of the laser beam was achieved using a dove prism, which was index matched to the backside of a glass slide containing the metal film, PE spacer, and immobilized NPs. A linear polarizer was used to create S-polarized (dipole oriented parallel to the film surface) or P-polarized (oriented normal to the film surface) illumination. DF mode was used to interrogate more accurately the distance-dependent nature of the SERRS signal from the NP-film gaps since DF illumination from above the sample surface gives equal illumination intensity at each NP-film gap distance. DF was chosen over TIR for distance dependence because TIR illumination intensity changes with distance above the metal film, and also, TIR mode contributes an added frequency-dependent field from the metal surface plasmon polariton, which shifts with increasing number of PE layers.[2] In DF mode, the laser beam was focused to a 100 μm diameter spot with a 1-inch convex lens and directed at the sample surface at 75° relative to the normal of the surface. In order to accommodate the beam being brought in from the side, we were forced to use a longer working distance, 50x 0.55 NA objective to acquire data. Here again, we used a linear polarizer in the beam path to provide S- and P-polarization.

For SERRS characterization, we typically imaged the NP-film gaps in two different modes: laser scattering and SERRS imaging mode. Laser scattering mode was used to identify single NPs near film as they scattered the incident laser illumination into the far field. For SERRS imaging mode, a long pass filter was used to block the laser light from the imaging light path and admit only Stokes-shifted light scattered by the NP-film gaps. Images were acquired within a region of interest on a grayscale CCD (Photometrics CoolSnap ES) that was defined to include only the field of view illuminated by the laser. SERRS intensities from single, film-coupled NPs were gathered by integrating the total CCD counts within a small region of interest containing a single NP scatterer, and subtracting the integrated counts from the same size region of interest, but located in a dark region of the image, to remove background signal. SERRS spectra were acquired using the SERRS imaging mode, but instead of directing light to the camera, light from single NPs was directed through a pinhole aperture (to cut down background signal) and into a spectrometer (Acton 2300SPI, CoolSnap HQ detector).

NP-film Polarization Response

Single NPs in close proximity to metal film scatter polarized light into the far field, as reported in Mock *et al.*[2] and shown in Figure 2A. This can be understood by considering that a NP near film induces an image dipole within the film. Consistent with an approximate image theory, the horizontal dipolar response of a nanoparticle close to the film tends to be reduced via interaction with its image, while the vertical dipole (perpendicular to the film) tends to be enhanced. The cancellation of the horizontal dipole response from a nanoparticle strongly coupled to its image, then, results in the characteristic doughnut-shaped point spread functions (PSFs) observed from the far-field scattering of white light by the NPs in close proximity to the film (Figure 2A and Mock *et al.*[2]).

When characterizing the SERRS response from NP-film gaps (Figure S4), we observed similar polarization responses with laser illumination as the case where white light was used. The NP-film gaps responded similarly to polarization in both TIR and DF modes of illumination. In each case, P-polarized laser illumination produced bright, doughnut-shaped laser scattering from single NPs near

film. In SERRS imaging mode, it was clear that every NP-film gap produced measurable SERRS signal. In most cases, this signal was also scattered through the vertical polarization dipole, as evidenced by the doughnut-shaped PSFs. However, we note that in some cases the doughnut PSF was not clearly evident, and we believe that vibrations in the imaging system, combined with perhaps a long "on" period of the observed blinking of the SERRS signal, may contribute to blurring of the PSF during the 10-seconds long SERRS image exposure time. As expected, NP-film gaps did not respond in a measureable way to S-polarized illumination. This was also the case in SERRS imaging mode.

References

(1) Domke, K.; Zhang, D.; Pettinger, B. *J. Am. Chem. Soc* **2006**, *128*, 14721-14727.

(2) Mock, J. J.; Hill, R. T.; Degiron, A.; Zauscher, S.; Chilkoti, A.; Smith, D. R. *Nano Lett.* **2008**, *8*, 2245-2252.

(3) Decher, G. *Science* **1997**, *277*, 1232.

(4) Marinakos, S. M.; Chen, S.; Chilkoti, A. *Anal. Chem.* **2007**, *79*, 5278-5283.

(5) Tronin, A.; Lvov, Y.; Nicolini, C. *Colloid & Polymer Science* **1994**, *272*, 1317-1321.

(6) Cant, N.; Zhang, H.-L.; Critchley, K.; Mykhalyk, T.; Davies, G.; Evans, S. *J. Phys. Chem. B* **2003**, *107*, 13557-13562.

(7) Johnson, P.; Christy, R. *Physical Review B* **1972**, *6*, 4370-4379.

(8) Bogatyrev, V.; Dykman, L.; Khlebtsov, B.; Khlebtsov, N. *Optics and Spectroscopy* **2004**, *96*, 128-135.

(9) Tcherniak, A.; Ha, J. W.; Dominguez-Medina, S.; Slaughter, L. S.; Link, S. *Nano Lett.* **2010**, *10*, 1398-1404.

(10) Ni, W.; Ambjo□rnsson, T.; Apell, S. P.; Chen, H.; Wang, J. *Nano Lett.* **2010**, *10*, 77-84.

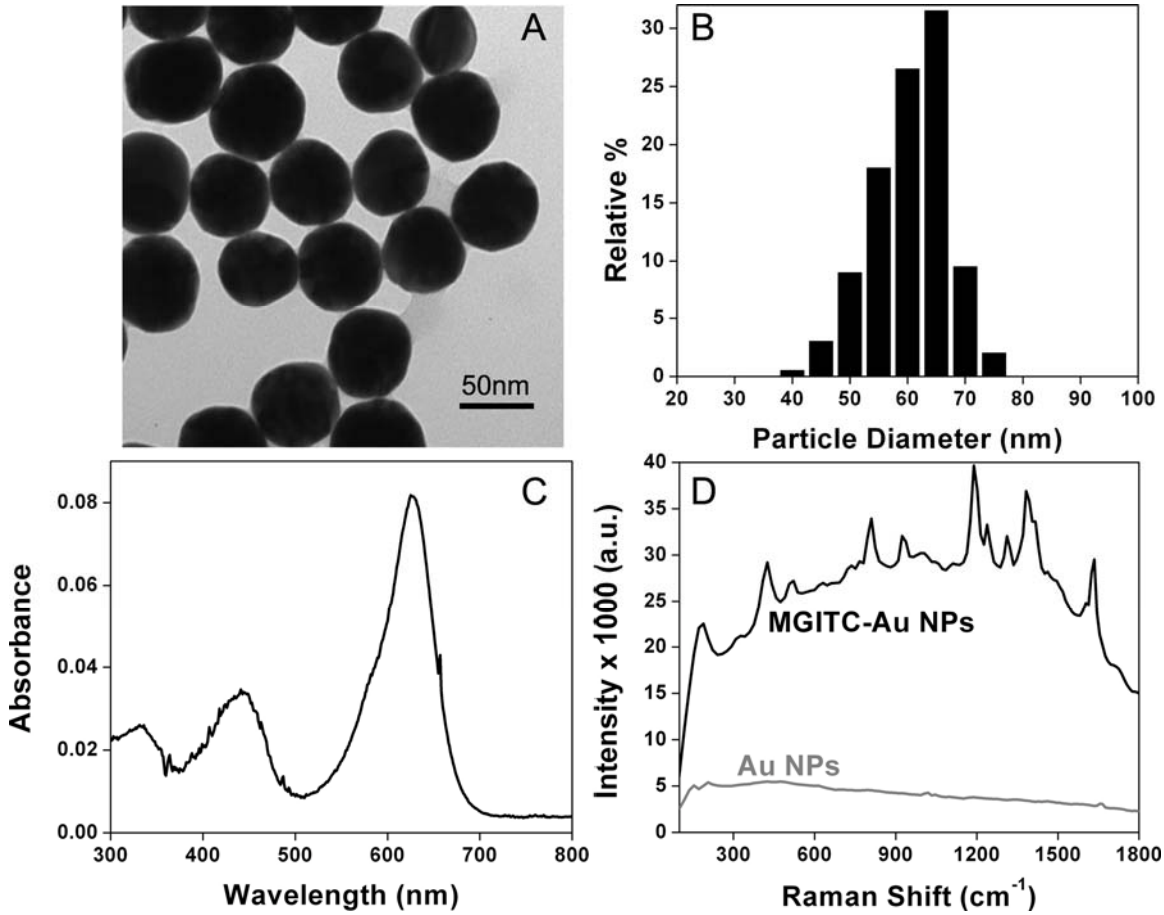

Figure S1. NP Characterization. A) shows a representative TEM image of the 60 nm BioPure™ nanoComposix gold NPs used in this study. B) shows a histogram representing the size variation of the NPs. C) shows the absorbance of 0.49 μM MGITC in water. D) shows a bulk SERRS spectrum from the MGITC functionalized NPs as compared to a bare Au NP control sample.

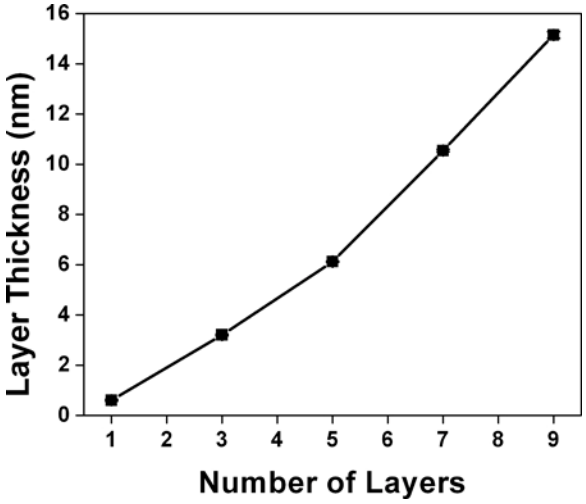

Figure S2. Average polyelectrolyte layer thickness, as measured by ellipsometry, versus number of deposited PE layers. Standard deviations are included in the plot, but are too small to see clearly. Thickness standard deviations were ≤ 0.5 Angstroms, except for the 9-layer sample, which had a thickness standard deviation of 1.3 Angstroms.

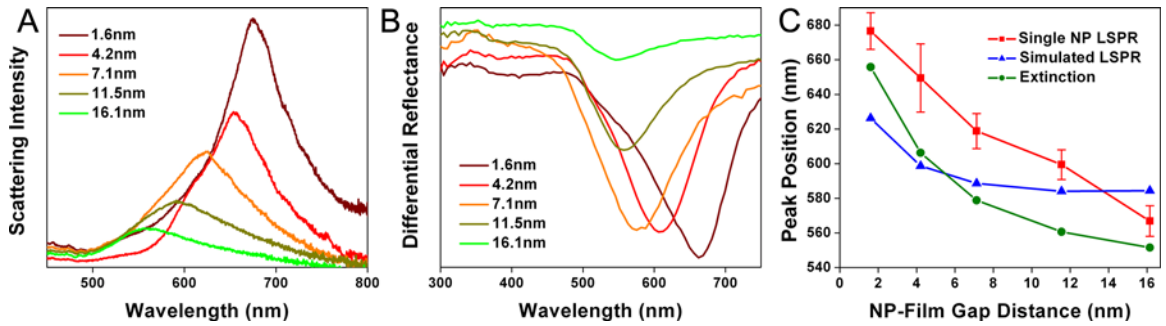

Figure S3. Plasmonic characterization of MGITC-Au NPs near gold film. A) shows representative single NP scattering spectra from NPs at various NP-film gap distances. B) shows extinction measurements from an ensemble of NPs near film at the various NP-film gap distances. C) shows the comparison of plasmonic shifts with NP-film gap distance from the single NP, extinction, and simulated data.

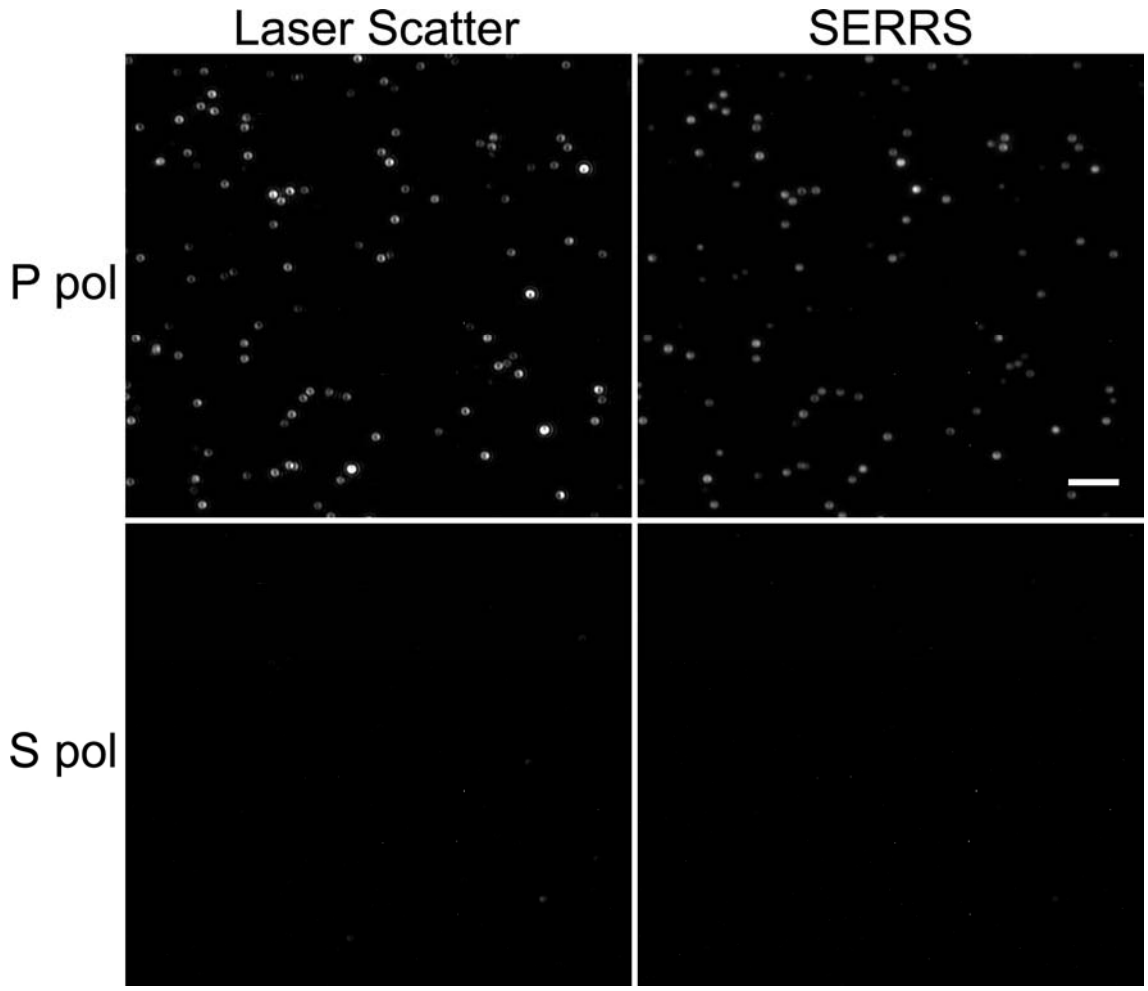

Figure S4. Response of NP-film gaps to polarization of incident beam. With P-polarized light, the NP-film gaps scattered laser illumination (top left) and, in SERRS imaging mode, produced measureable SERRS (top right). These images show a wide field of view so as to demonstrate that essentially every NP-film gap identified in the laser scattering image (top left) produces SERRS (top right) in SERRS imaging mode. With S-polarized light, minimal laser scattering (bottom left) or SERRS (bottom right) is detected. S-polarized images were taken with identical exposure times as the corresponding P-polarized images. The contrast in each of the four images is set to be exactly the same for direct visual comparison of intensity levels. Scale bar = 5 μm.